Single curved fiber sedimentation under gravity

Xiaoying Rong , Dewei Qi , Guowei He , JunYong Zhu , Tim Scott

Abstract

Dynamics of single curved fiber sedimentation under gravity are simulated by using the lattice Boltzmann method. The results of migration and rotation of the curved fiber at different Reynolds numbers are reported. The results show that the rotation and migration processes are sensitive to the curvature of the fiber.

Keywords: Lattice Boltzmann simulation; Fiber suspensions; Curved fibers

1. Introduction

Understanding of migration and aggregation of curved and flexible fibers is important for the papermaking process. Fiber motion is directly related to flocculation and dispersion. With increasing operation speed, the inertia of fibers in the headbox and forming section cannot be ignored.

Particle suspension with zero or small Reynolds numbers has been studied experimentally and numerically. Segré and Silberger [1], Karins and Mason [2] observed that the equilibrium position of a neutrally buoyant particle in Poiseuille flow is located between the wall and the tube axis due to inertial effects. Feng, Hu and Joseph [3] investigated the motion of single circular and elliptic particle settling in a Newtonian fluid. It was found that the center of the channel is the equilibrium position regardless of the initial position of the particle. With inertia, the particle experiences five different regimes of motion: steady motion with and without overshoot, weak, strong and irregular oscillations. An elliptic particle always turns its long axis perpendicular to the fall and drifts to the centerline of the channel during sedimentation.

Huang et al. [4] simulated single circular cylinder in Coutte and Poiseuille flows of viscoelastic fluids. The simulation results numerically proved that the equilibrium position of slightly buoyant particles migrating in Newtonian fluids is different to that in viscoelastic fluids. In the Coutte flow, the equilibrium position of a slightly buoyant particle is nearer the centerline of the channel in a viscoelastic fluid than in a Newtonian fluid. In the Poiseuille

flow, the equilibrium position of the same particle is farther away from the centerline of the channel in a viscoelastic fluid than in a Newtonian fluid.

Three-dimensional rotation and translation of non-spherical particles including ellipsoids and cylinders at small aspect ratios were studied by Qi [5–7]. Qi [7] found that when sedimenting at near zero Reynolds number, the long axis of ellipse particle turns vertically. It turns horizontally as the Reynolds number increases. Migration and orientation behavior of single and multiple ellipsoidal particles in a planar Poiseuille flow were investigated by Qi et al. [8]. They showed that at a steady state, multi-particles with elliptical shape have higher probability to be oriented along the streamline than across them. Multiple-particles tend to locate between the wall and the center line of the channel. When a single particle is slightly denser than the fluid, it moves towards the wall. When the particle density is large enough, it moves towards the center.

The aspect ratio of non-spherical axisymmetric particle affects the orientation and settling velocity [9]. As shown in the research, in Newtonian fluid, single axisymmetric fiber turns to be horizontal regardless of its aspect ratio. The single fiber with higher aspect ratio reaches the maximum settling velocity faster than the fiber with smaller aspect ratio. Fibers with different aspect ratios have the same terminal settling velocity if the fibers have same density and diameter.

Experimental and numerical studies [10–12] of the sedimentation of fiber suspensions revealed that in a multiple-particle system, the orientation and sedimentation velocity of non-spherical, axisymmetric particles are strongly hindered by particle interactions. At low Reynolds numbers, most of the fibers are aligned in the direction of gravity with occasional "flips". The fiber clumps settle faster than isolated vertical fibers.

In pulp and paper processes, fibers may be curved rather than straight. Experimentation showed that the rotation of flexible fibers in shear flow at diluted region appears springy, snake-turn and S-turn orbits. The rotation of slightly curved fibers and the viscosity of curved fiber suspensions are different from those of straight fibers [13]. Qi [14] studied flexible fiber in a shear flow at finite Reynolds numbers. A flexible fiber was modeled as a chain of spheres with different stiffnesses. The rotation of a flexible fiber changes from rigid rotation to springy, then the more flexible fiber shows an S-turn finally. Considering inertial effects, the rotation is slowed down due to streamline separation.

Some fibers, especially the recycled fibers, have some permanent deformations, which make fibers slightly curved. The suspension and sedimentation behavior of curved fibers in a Newtonian fluid are certainly different from those of axisymmetric fibers. In this study, curved fibers are shaped as an arc. The curved fibers settle under gravity is numerically simulated by lattice Boltzmann method. Fibers with the same aspect ratio and different curl indices are studied to characterize the dynamic behavior of curved fiber sedimentation.

2. Numerical methods

Navier–Stokes equations are solved directly by lattice Boltzmann method. This method has been successfully applied to simulate the interaction between fluid and solid particles [7,15–17]. In the lattice Boltzmann (LB) method, fluid particles are divided into discrete nodes. The fluid particles move to their nearest neighbors along the links with unit spacing in each unit time step.

In the lattice Boltzmann (LB) method, fluid particles reside on the lattice nodes and move to their nearest neighbors along the links with unit spacing in each unit time step. The lattice Boltzmann equation with Bhatanagar–Gross–Krook (BGK) single relaxation time, is given by

$$f_\sigma(\vec{x}_i + \vec{e}_\sigma, t+1) = f_\sigma(\vec{x}_i, t) - \frac{1}{\tau}[f_\sigma(\vec{x}_i, t) - f_\sigma^{eq}(\vec{x}_i, t)], \tag{1}$$

where $f_\sigma(\vec{x}, t)$ is the fluid particle distribution function for particles with velocity $\vec{e}_\sigma$ at position x and time t, $f_\sigma^{eq}(\vec{x}, t)$ is the equilibrium distribution function and τ is the single relaxation time.

The simulation described in this paper is performed using the D3Q15 model. It possesses a rest particle state, six links with the nearest neighbors, and eight links with the next nearest neighbors. Periodic boundary conditions in the flow direction with bounce back on the solid nodes are used. $f_\sigma^{eq}(\vec{x}, t)$ is taken as

$$f_\sigma^{eq}(\vec{x}, t) = \omega_\sigma \rho_f \left\{1 + 3(\vec{e}_\sigma \cdot \vec{u}) + \frac{9}{2}(\vec{e}_\sigma \cdot \vec{u})^2 - \frac{3}{2}(\vec{e}_\sigma \cdot \vec{e}_\sigma)\right\}, \tag{2}$$

where ρ_f is the density of the fluid, $\vec{u}$ is the velocity. $\sigma = 1$ represents the particles moving to the nearest neighbors,

$\sigma = 2$ represents the particles moving to the second nearest neighbors, $\sigma = 0$ represents the particles rest at the nodes. The weight coefficient ω_σ depends on the discrete velocity set $\vec{e}_\sigma$ and dimensions of space. In the D3Q15 model, the discrete velocity set is

$$\vec{e}_\sigma = \begin{cases} (0,0,0), & \sigma = 0 \\ (\pm 1,0,0) \quad (0,\pm 1,0) \quad (0,0,\pm 1), & \sigma = 1 \\ (\pm 1,\pm 1,\pm 1), & \sigma = 2 \end{cases} \tag{3}$$

and the weight coefficient is

$$\omega_\sigma = \begin{cases} \dfrac{2}{9}, & \sigma = 0 \\ \dfrac{1}{9}, & \sigma = 1 \\ \dfrac{1}{72}, & \sigma = 2. \end{cases} \tag{4}$$

The mass density ρ_f and momentum density $\rho_f \vec{u}$ are given by,

$$\rho_f = \sum_\sigma f_\sigma \qquad \rho_f \vec{u} = \sum_\sigma f_\sigma \vec{e}_\sigma . \tag{5}$$

In a widely used class of models, the kinematic viscosity ν is related to the relaxation time τ for convergence, is given by:

$$\nu = \frac{1}{3}\left(\tau - \frac{1}{2}\right). \tag{6}$$

When the particles are suspended in the fluid, the fluid particles and solid particles collide. The detailed method which has been reported [7,15,17] is not repeated here.

3. Results and discussions

The curved fiber and its corresponding parameters are shown in Fig. 1. The curl index is defined as $C = \frac{L}{L'} - 1$ [18]. L' is the end-to-end length of the curved fiber, L is the contour length of the curved fiber. The aspect ratio of the fiber is given by $\frac{L}{d}$. d is the diameter of fiber. X' and Z' are the primary axes of the curved fiber. X and Z are the coordinates of simulation channel.

A single curved fiber is assumed to settle in an infinitely long vertical channel filled with the Newtonian fluid along the Z-direction. The gravity is the only driving force for the settling. Once the initial position of the fiber is given, the flow is determined by several parameters: ρ_s, ρ_f, L, d, C, where ρ_s is the density of solid fiber, ρ_f is the density of fluid. The density ratio is defined as $\frac{\rho_s}{\rho_f}$.

Sedimentation of two curved fibers with different curl indices and one straight fiber with flat ends settling under gravity are studied (Fig. 2). Fibers studied are at the same aspect ratio. The Reynolds number is calculated by $Re = \frac{VL'}{\nu}$, where, V is the average terminal velocity of fiber, ν is the kinematical viscosity of fluid. For straight fiber, $L' = L$. When a fiber settles under gravity, the mean terminal velocity and Reynolds number are controlled by the density ratio.

A simulation box of $140 \times 60 \times 300$ lattice units is used. In this scale, the length of the fiber is $L = 40$ and the diameter is $d = 8$ which give the fiber an aspect ratio of 5. The mass center of curved or straight fibers is placed at $0.3W$ in the X-direction. The fiber settles along the Z-direction. $W = 140$ is the width of the channel. Y-direction is a periodical boundary. The curl indices of curved fiber are set as 0.2 and 0.57. Two different density ratios are 1.01 and 1.05.

3.1. Lateral migration

It has been proven in the many studies that the centerline of the channel is an equilibrium position of settling. The curved and straight fibers will reach the center of the channel regardless of their initial positions. However, the different initial positions of curved fibers may result in different trajectories of migration (Fig. 3).

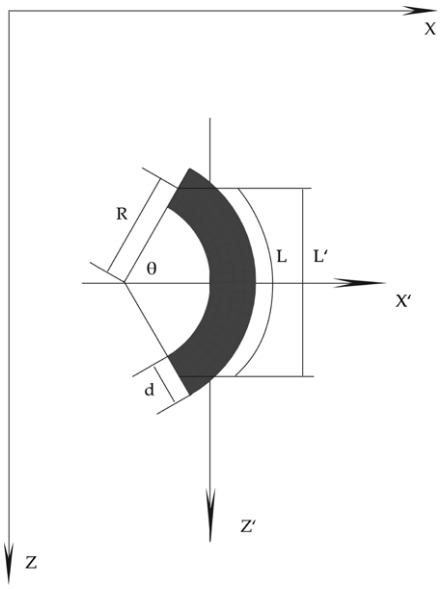

Fig. 1. Curved fiber and its parameters.

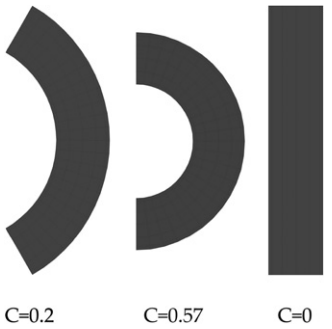

Fig. 2. Two curved fibers and one straight fiber.

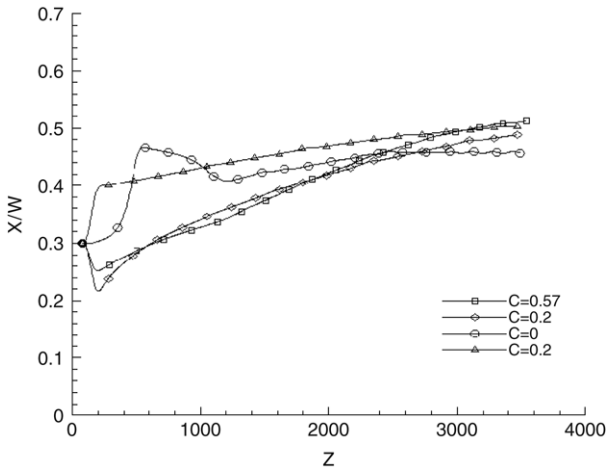

Fig. 3. Lateral migration of curved and straight fibers at the density ratio of 1.05, the Reynolds number of the curved fibers is $Re = 31.2$, the Reynolds number of the straight fiber is $Re = 37.7$. The diamond and square symbols represent the curved fibers with their concave sides facing the left wall. The triangle symbol represents the curved fiber with its convex facing the left wall. The X-axis is the position of fiber mass center.

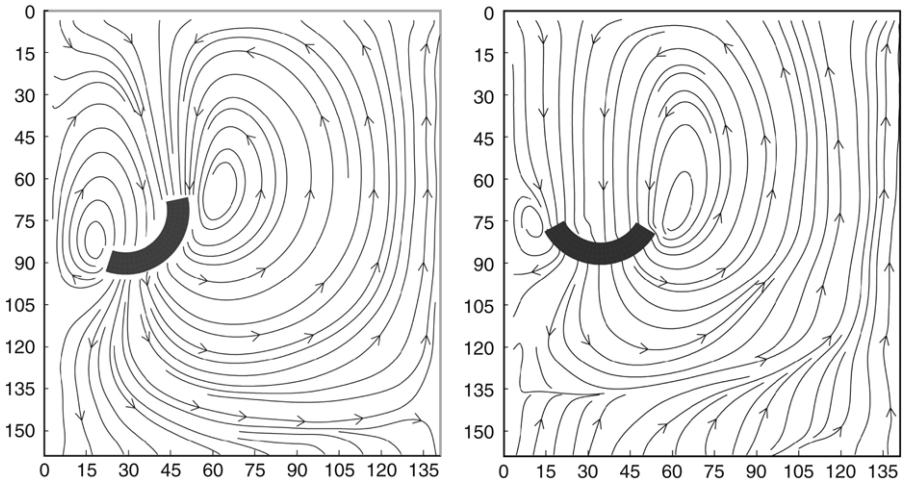

Fig. 4. (Left): Flow streamlines and the curved fiber with the curl index of $C = 0.2$ and the density ratio of 1.05 at the time step of 3000. (Right): Flow streamlines and the curved fiber with the curl index of $C = 0.2$ and the density ratio of 1.05 at the time step of 8000.

In the first case of $C = 0.2$, the curved fiber with the density ratio of 1.05 is released from the initial position (42, 30, 80) with zero initial velocity. The initial position is not in the center of the channel. The concave side of the fiber faces the left wall. The curved fiber shows a lateral migration towards the wall first, and it is repelled towards the center of the channel later. This motion can be clearly shown in the figure with flow streamlines. The curved fiber generates two vortices at the ends of the fiber due to the curvature and rotation of the fiber. The left vortex is more intense (Fig. 4, Left). The pressure difference moves the fiber towards the wall. After the curved fiber turns itself perpendicular to the gravity, the intensity of the left vortex, as shown in Fig. 4 (Right), is reduced and the wall pushes the fiber towards the center of the channel.

It is necessary to determine whether the initial direction of the curved fiber has an influence on the migration and rotation. For this purpose, a curved fiber with the curl index of $C = 0.2$ and the density ratio of 1.05 is placed at the same lateral position. The only difference is that the concave side of the fiber faces the channel center. The results show that this curved fiber has no initial movement towards the wall and the fiber moves towards the center of the channel monotonically. It is obvious that the initial direction of the curved fiber will influence the trajectory behavior even when they are placed at the same initial position.

To compare the influence of curvature to migration and rotation, a curved fiber with the curl index of $C = 0.57$ and the density ratio of 1.05 is studied. In this case, the curved fiber is placed with its concave faces the left wall. With a higher curl index, the curved fiber shows less movement towards the wall before it starts to move towards the center of channel. On the contrary, the straight fiber at same density ratio and aspect ratio moves towards the center of the channel without moving towards the wall first.

3.2. Rotation

Studies showed that, without the influence of inertia, a non-spherical particle will fall along the stream under gravity with its long axis. While the inertia effect is considered, a non-spherical particle will rotate itself until its long axis becomes horizontal. In this study, the curved and straight fibers sediment under gravity, and the inertia effect is considered. The rotation angle is defined as the absolute value of the angle between Z-axis of the fiber and Z-axis of the simulation box.

The results show that the curved fiber always turns itself perpendicular to the gravity at the studied Reynolds numbers. At the density ratio of 1.05, the Reynolds number of the curved fiber reaches $Re = 31.2$. The curved fiber turns quickly to be horizontal while the straight fiber takes a longer time to turn itself to be horizontal (Fig. 5). The curved fibers with different curl indices show the same tendency of rotation. With a larger curl index, the fiber rotates faster than the one with a smaller curl index. This can be explained by the different curvatures associated with different moments of inertia. The curved fiber with the larger curl index induces a lower moment of inertia about its rotation axis than the straight one (Fig. 6).

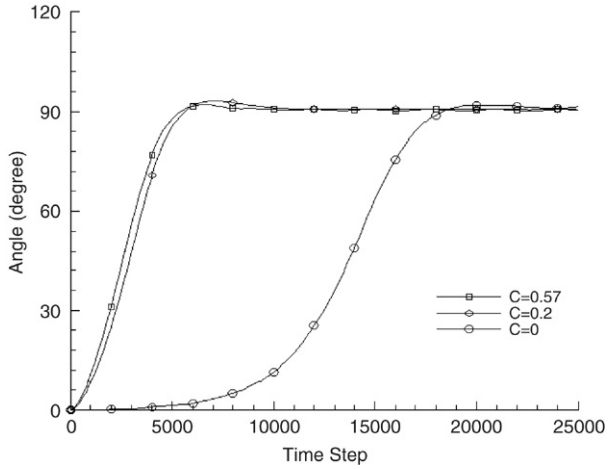

Fig. 5. Rotations of curved and straight fibers at the density ratio of 1.05. Here, the concave side of the fiber faces the left wall.

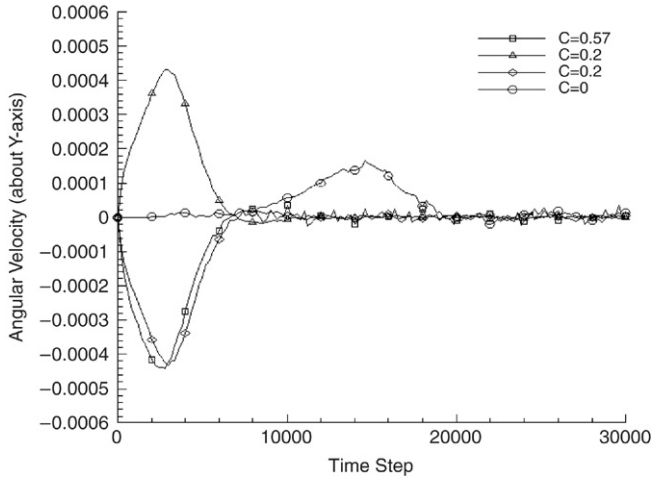

Fig. 6. Angular velocities of curved fiber and straight fiber at the density ratio of 1.05. Here, the triangle symbol represents the curved fiber with the curl index of $C = 0.2$ and with its convex facing the left wall, the diamond symbol represents the curved fiber with the curl index of $C = 0.2$ but with its concave side facing the left wall.

The angular velocities shown in Fig. 6 also demonstrates that the initial direction and curvature of fiber result in different rotations. When the concave side of the curved fiber faces the left wall, the fiber turns clockwise to be perpendicular to the gravity. When the convex of curved fiber faces the left wall, the fiber turns counter-clockwise to be perpendicular to the gravity. Straight fiber turns counter-clockwise as well. The curvature and initial direction of the curved fiber have significant influence on rotation.

3.3. Settling velocity

The sedimentation of non-spherical particles differs quantitatively from the sedimentation of spherical particles. As shown in this study, the sedimentation of curved fiber differs from that of straight fiber.

At the same density ratio, the terminal settling velocities of curved fibers at different curl indices are different. Fig. 7 shows the settling velocities of curved fibers at the density ratio of 1.01. The settling velocity increases rapidly when the fiber is just released. The fiber with a higher curl index can reach higher maximum settling speed. The settling velocity becomes stable when the fiber is horizontal and close to the center of the channel. The fiber with a larger curl index has smaller overshooting speed as shown in Fig. 7. The terminal velocity of the fiber with a larger

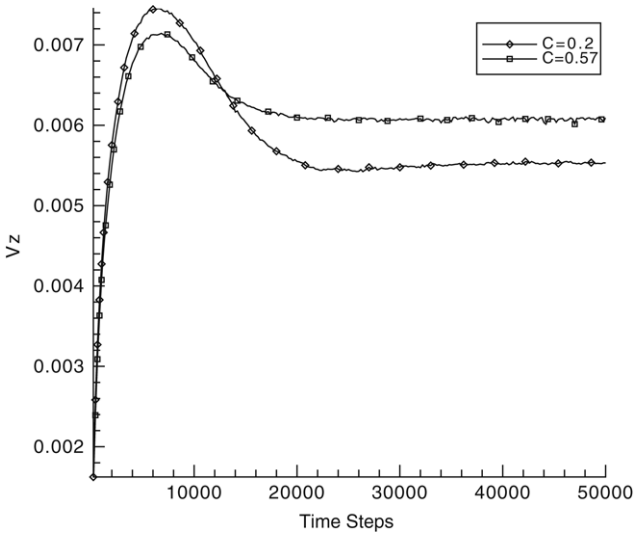

Fig. 7. The terminal velocities of curved fibers at the density ratio of 1.01. The Reynolds number of curved fiber at $C = 0.57$ is $Re = 11.7$. The Reynolds number of curved fiber at $C = 0.2$ is $Re = 9.8$. The concave side faces the left wall.

curl index is higher than the one with smaller curl index. This may be explained by the drag force on different shapes of fiber.

4. Conclusions

Rotation and migration of curved and straight fibers while settling under gravity are studied by the lattice Boltzmann method. It is found that the migration and rotation of the fiber are sensitive to the curvature. The curved fiber always turns its long body perpendicular to the direction of gravity at all the Reynolds numbers tested. A fiber with a smaller curl index reaches the terminal velocity slower than the fiber with a larger curl index. However, the terminal velocity of the fiber with a larger curl index is higher than the fiber with a smaller curl index. The fiber with higher curl index also shows smaller overshooting during settling.

It is demonstrated that the initial direction of the fiber affects the migration trajectory. When the concave side of the fiber is close to the wall, the fiber initially moves towards the wall due to the pressure difference. After the vortex intensity is reduced, the wall effect pushes the fiber to the center of the channel. The curved fiber turns clockwise to be horizontal under this condition. When the concave side of fiber faces the channel center, the fiber moves towards the center monotonically and turns itself counter-clockwise to be horizontal. In short, the initial direction of the concave fiber will influence the trajectory of rotation and migration even though they have the same initial positions.

Acknowledgement

This study is partially supported by USDA Forest service, Fiber Product Lab.

References

[1] G. Sigré, A. Silberberg, Radial, Poiseuille flows of suspensions, Nature 189 (1961) 209.
[2] A. Karins, S.G. Mason, Particle motions in sheared suspensions. XIX. Viscoelastic media, Trans. Soc. Rheol. 10 (1966) 571.
[3] J. Feng, H.H. Hu, D.D. Joseph, Direct simulation of initial value problems for the motion of solid bodies in a Newtonian fluid, Part 1, Sedimentation J. Fluid Mech. 261 (1994) 95.
[4] P.Y. Huang, J. Feng, H.H. Hu, D.D. Joseph, Direct simulation of the motion of solid particles in Couette and Poiseuille flows of viscoelastic fluids, J. Fluid Mech. 343 (1997) 73.
[5] D.W. Qi, Non-spherical colloidal suspensions in three-dimensional space, Internat. J. Modern Phys. C 80 (1997) 98.
[6] D.W. Qi, Computer simulation of coating suspensions, in: Tappi Fundamental Coating Symposium, 1997, p. 201.
[7] D.W. Qi, Lattice-Boltzmann simulations of particles in non-zero-Reynolds-number flow, J. Fluid Mech. 385 (1999) 41.
[8] D.W. Qi, L.S. Luo, R. Aravamuthan, W. Strieder, Lateral migration and orientation of elliptical particles in Poiseuille flows, J. Stat. Phys. 107 (2002) 101.

[9] J.Z. Lin, X. Shi, Z.J. You, Effects of the aspect ratio on the sedimentation of fiber in Newtonian fluids, Aerosol Sci. 34 (2003) 909.
[10] B. Herzhaft, E. Guazzelli, Experimental investigation of the sedimentation of dilute fiber suspension, Phys. Rev. Lett. 77 (2) (1996) 290.
[11] B. Herzhaft, E. Guazzelli, Experimental study of the sedimentation of dilute and semi-dilute suspensions of fibres, J. Fluid Mech. 384 (1999) 133.
[12] M.B. Mackaplow, E.S.G. Shaqfeh, A numerical study of the sedimentation of fibre suspensions, J. Fluid Mech. 376 (1998) 149.
[13] O.L. Forgacs, S.G. Mason, Particle motions in sheared suspensions: X. Orbits of flexible threadlike particles, J. Colloid Sci. 14 (1959) 473.
[14] D.W. Qi, A new method of simulations of flexible particles in finite Reynolds number flows, in: International Conference of Mesoscopic Methods in Engineering and Science; AIChE Annual Conference, Austin, Texas, 2004.
[15] C.K. Aidun, Y. Lu, E. Ding, Direct analysis of particulate suspensions with inertia using the discrete Boltzmann equation, J. Fluid Mech. 373 (1998) 287.
[16] A.J.C. Ladd, Numerical simulations of particle suspensions via a discretized Boltzmann equation. Part 1. Theoretical foundation, J. Fluid Mech. 271 (1994) 285.
[17] Y.D. Qian, D. d'Humieres, P. Lallemand, Lattice BGK models for Navier–Stokes equation, Europhys. Lett. 17 (1992) 479.
[18] D.H. Page, R.S. Seth, B.D. Jordan, M.C. Barbe, Curl, crimps, kinks and microcompressions in pulp fibres: Their origin, measurement and significance, in: Proc. 8th Fund. Res. Symp. Fundamentals of papermaking, 1, Oxford UK, 1985, p. 183.